Research Article | Vol. 31, No. 14 / 3 Jul 2023 / Optics Express 23027
Optics EXPRESS

High-resolution self-corrected single-pixel imaging through dynamic and complex scattering media

LINA ZHOU,[1] YIN XIAO,[1] AND WEN CHEN[1,2,*]

[1]Department of Electronic and Information Engineering, The Hong Kong Polytechnic University, Hong Kong, China
[2]Photonics Research Institute, The Hong Kong Polytechnic University, Hong Kong, China
*owen.chen@polyu.edu.hk

Abstract: Imaging with single-pixel detectors becomes attractive in many applications where pixelated detectors are not available or cannot work. Based on a correlation between the probing patterns and the realizations, optical imaging with single-pixel detector offers an indirect way to recover a sample. It is well recognized that single-pixel optical imaging through dynamic and complex scattering media is challenging, and dynamic scaling factors lead to serious mismatches between the probing patterns and the realizations. In this paper, we report self-corrected imaging to realize high-resolution object reconstruction through dynamic and complex scattering media using a parallel detection with dual single-pixel detectors. The proposed method can supervise and self-correct dynamic scaling factors, and can implement high-resolution object reconstruction through dynamic and complex scattering media where conventional methods could not work. Spatial resolution of 44.19 μm is achieved which approaches diffraction limit (40.0 μm) in the designed optical setup. The achievable spatial resolution is dependent on pixel size of spatial light modulator. It is experimentally validated that the proposed method shows unprecedented robustness against complex scattering. The proposed self-corrected imaging provides a solution for ghost recovery, enabling high-resolution object reconstruction in complex scattering environments.

1. Introduction

The object recovery is generally dependent on pixelated sensor arrays, e.g., charge-coupled device, which revolutionized the imaging field. However, pixelated detectors could not be available or expensive in some applications, when non-visible light sources are used or weak light intensities need to be recorded. An imaging scheme with single-pixel detector has emerged to overcome the challenges [1–5]. Optical imaging with single-pixel detection, e.g., ghost imaging (GI) [6–20], has attracted much attention due to its remarkable characteristics. The theory of GI originated from quantum [6]. It was subsequently verified that classical light source can also be exploited to retrieve ghost [8–20]. The GI acquires spatial information via a correlation between time-varying probing patterns and the realizations [8–10]. When the probing patterns and light intensities measured by single-pixel detector are correlated, a ghost image could be recovered. The advance in spatial light modulator (SLM) has opened up a new research perspective for GI, giving rise to much research on computational GI. Different GI methods have been developed to enhance quality of the reconstructed samples, e.g., differential [21], normalized [22] and Gerchberg-Saxton-like [23]. Much effort has also been made to increase the speed of data recording and computing [24–32] using compressed sensing [24–26], fast switching devices (e.g., digital micromirror device [27] and light emitting diode [28]) and deep learning [30–32]. The GI not only shows enhanced denoising performance, but also enables fast measurements. The GI has also been demonstrated to have an advantage of imaging through scattering media [11,12].

#489808 https://doi.org/10.1364/OE.489808
Journal © 2023 Received 16 Mar 2023; revised 21 Apr 2023; accepted 2 May 2023; published 26 Jun 2023

Optics EXPRESS

Much research interest has been triggered, e.g., terahertz [33–38]. However, single-pixel imaging through dynamic and complex scattering media remains an open question. The imaging has been applied in static and micro dynamic scattering media [39–42]. However, the performance of GI is still limited in dynamic and complex scattering environments. This is attributed to dynamic scaling factors induced by the evolution of scattering environment. The dynamic scaling factors give rise to serious mismatches between the probing patterns and the measurements, resulting in a failure of conventional methods. Therefore, it is well recognized that high-resolution single-pixel imaging through dynamic and complex scattering media is challenging.

In this paper, we propose self-corrected imaging with dual single-pixel detectors to realize high-resolution imaging through dynamic and complex scattering media. A reference beam is introduced to monitor and correct the change of scaling factors. The mismatches, i.e., between illumination (probing) patterns and the realizations, induced by dynamic and complex scattering media can be corrected in real time. It is experimentally demonstrated that high-resolution samples can be recovered by using a rectified correlation algorithm. This is the first attempt to apply a parallel detection with dual single-pixel detectors to implement self-correction of optical imaging through dynamic and complex scattering media. The proposed method enables high-resolution imaging through dynamic and complex scattering media where conventional methods could not work. The proposed method shows high robustness against dynamic and complex scattering media.

2. Principle

A schematic experimental setup is shown in Fig. 1. A green laser beam (CrystaLaser, CL-2000) with wavelength of 532.0 nm and power of 25.0 mW is expanded and collimated to illuminate an amplitude-only SLM (Holoeye LC-R720) with pixel size of 20.0 μm. A series of designed illumination patterns with 128×128 pixels are sequentially embedded into the SLM. Then, one beam illuminates a sample, e.g., USAF 1951 resolution target (Thorlabs, R3L3S1N), and then propagates through dynamic and complex scattering media. Another beam propagates through dynamic and complex scattering media without an interaction with the sample. 6000 ml pure water is placed in water tank (10.0 cm (L) × 30.0 cm (W) × 30.0 cm (H)) for each experiment. In this study, 300 ml pure water is first placed in the funnel, and then different volumes of skimmed milk are directly added into the funnel for each experiment. A stirrer with the maximum speed of 1200 revolutions per minute (rpm) is used to generate dynamic environments. The object and reference waves are recorded by single-pixel silicon photodiodes (Thorlabs, PDA100A2). In Fig. 1, the funnel is placed away from the reference beam by 12.0 cm, and the stirrer is placed away from the object beam by 12.0 cm. The single-pixel detectors and SLM are synchronized by data acquisition device (Smacq, USB-5210) and purpose-built Labview program. The time interval to display each illumination pattern in the SLM is 100 ms in this study, and 40000 illumination patterns are sequentially embedded and displayed.

A series of illumination patterns $P_i(x, y)(i = 1,2,3,\ldots,40000)$ with 128×128 pixels are generated to satisfy that sum of all pixel values in each illumination pattern, i.e., *cons*, is the same as described by

$$\begin{aligned} \int P_i(x, y)dxdy &= cons \\ &= \mathrm{FFT}\{P_i(x, y)\}_{(0,0)}, \end{aligned} \tag{1}$$

where FFT denotes fast Fourier transform. It is given in Eq. (1) that zero-frequency component of Fourier spectrum is equal to the sum of all pixel values of pattern $P_i(x, y)$. A schematic of the proposed algorithm is shown in Fig. 2. The input is a random matrix, and is Fourier transformed to get spectrum q. A constraint is applied in Eq. (1) to obtain an updated Fourier spectrum q'. By applying inverse Fourier transform, a pattern can be generated, satisfying $\sum \tilde{P} = cons$. Since the updated pattern $\tilde{P}$ may contain negative values, a non-negative constraint could be applied

Optics EXPRESS

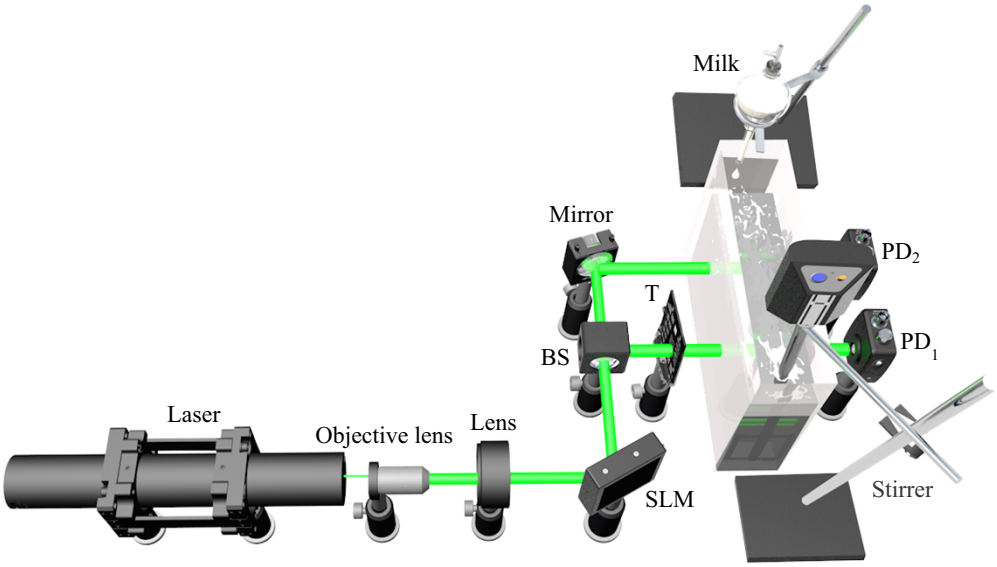

Fig. 1. A schematic experimental setup for the proposed imaging through dynamic and complex scattering media. SLM: spatial light modulator; BS: beam splitter cube; PD: single-pixel detector; T: target (sample).

to adjust. Therefore, a series of illumination patterns can be generated, when this modified algorithm is repeatedly used.

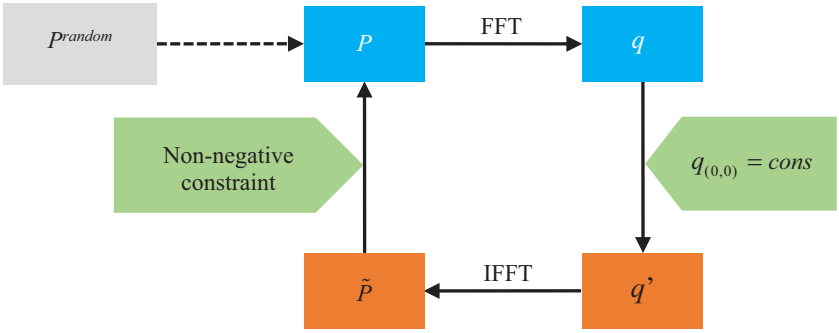

Fig. 2. A schematic of the generation of illumination patterns. P^{random}: a random matrix; FFT: fast Fourier transform; q: Fourier spectrum of P; q': an updated Fourier spectrum; IFFT: inverse fast Fourier transform; $\tilde{P}$: an updated pattern.

When the generated pattern is embedded into SLM, there might be a slight fluctuation in the sum of the generated pattern and this influence can be omitted in practice [13]. The parallel detection with dual single-pixel detectors is developed to synchronously collect light intensities. The reference wave propagates through dynamic and complex scattering media, and the object wave illuminates a sample $O(x, y)$ before propagating through dynamic and complex scattering media. Finally, light intensities at the two wave paths are recorded by single-pixel detectors. In a static scattering environment, when the ith illumination pattern is used, light intensities I_i

Optics EXPRESS

recorded in the reference beam path could be simply described by

$$I_i = \int P_i(x,y)dxdy. \tag{2}$$

In dynamic and complex scattering media, light intensities recorded in the reference beam path could be described by

$$\tilde{I}_i = k_i \int P_i(x,y)dxdy, \tag{3}$$

where k_i denotes a dynamic scaling factor. The light intensities $\hat{I}_i$ recorded in the object beam path could be described by

$$\hat{I}_i = \tilde{k}_i \int P_i(x,y)O(x,y)dxdy, \tag{4}$$

where $\tilde{k}_i$ denotes a dynamic scaling factor in the object beam path when the ith illumination pattern is used.

The scaling factors are corrected for each recording, and the following assumption can be used when separation distance between the reference beam and object beam is short.

$$k_i \approx \tilde{k}_i. \tag{5}$$

By applying this assumption, we have

$$\hat{I}_i = \frac{\tilde{I}_i}{\sum P_i(x,y)} \int P_i(x,y)O(x,y)dxdy. \tag{6}$$

Therefore, the sample can be reconstructed by using a rectified correlation algorithm [43].

$$O(x,y) = \left\langle \left(\frac{\hat{I}_i}{\tilde{I}_i} \sum P_i(x,y) - \left\langle \frac{\hat{I}_i}{\tilde{I}_i} \sum P_i(x,y) \right\rangle \right) (P_i(x,y) - \langle P_i(x,y) \rangle) \right\rangle, \tag{7}$$

where $\langle \cdots \rangle$ denotes an ensemble average over the total number of realizations. As can be seen in Eq. (7), the rectified correlation algorithm is applicable with random patterns. In order to directly monitor dynamic change of scaling factors, designed patterns with the same sum are applied. $\sum P_i(x,y)$ is designed to be a constant, and it can be omitted in image recovery. It is worth mentioning that the rectified correlation algorithm in Eq. (7) is also applicable in optical imaging through static or micro dynamic scattering media, e.g., ground diffusers, diaphragms, smoke, fog and biological tissues. In addition, the number of realizations is not needed to be increased in the proposed method owing to the setup design with dual single-pixel detectors, when optical imaging through dynamic and complex scattering media is conducted.

3. Experimental results and discussion

3.1. Proof-of-principle experiment

USAF 1951 resolution target and eight 3D-printed transparent samples are tested. Figures 3(a1)–3(a3) and 3(b1)–3(b3) show the reconstructed targets using the proposed optical imaging and conventional GI through dynamic and complex scattering media, respectively. The dynamic and complex scattering media are formed by using 10 ml, 4 ml and 5 ml milk respectively corresponding to Group 1, Group 2 and Group 3 of the USAF target, and the stirrer kept operating at 500 rpm over 4000 seconds. As can be seen in Figs. 3(a1)–3(a3), the change of scaling factors induced by dynamic and complex scattering media is corrected, and the recovered samples are of high quality. However, it is impossible for conventional GI to retrieve any information about the target, as shown in Figs. 3(b1)–3(b3). This is attributed to dynamic scaling factors aroused

Optics EXPRESS

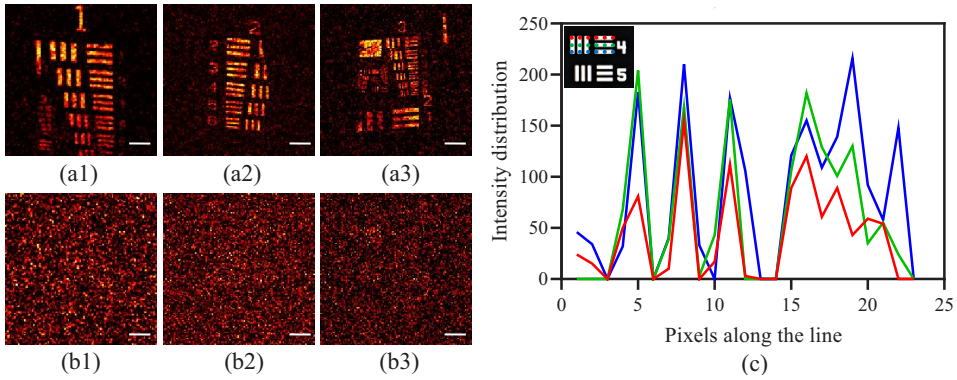

Fig. 3. Reconstruction results of a resolution target: (a1)-(a3) Group 1, Group 2 and Group 3 of the resolution target recovered by the proposed method respectively using 10 ml, 4 ml and 5 ml milk to be continuously dropped into water tank and a stirrer at 500 rpm. (b1)-(b3) Group 1, Group 2 and Group 3 of the resolution target recovered by using GI. (c) Intensity distributions of one-dimensional profiles in the recovered resolution target (i.e., element 4 of Group 3) using the proposed method. The inset on the top left corner of (c) is original image only for better visualization and marking. Scale bar: 1 mm.

by dynamic and complex scattering media. As can be seen in Fig. 3(a3), the finest structure identified in the recovered resolution target is element 4 of Group 3 (44.19 μm), approaching diffraction limit (see Fig. S1 in Supplement 1 for details).

To better visualize the achievable spatial resolution, one-dimensional profiles denoted by red, green and blue lines in the resolution target (i.e., element 4 of Group 3) are shown in Fig. 3(c). Three peaks can be clearly observed corresponding to three vertical bars in element 4 of Group 3. The detailed intensity distributions are given in Figs. 4(a) and 4(b). As can be seen in Figs. 4(a) and 4(b), the vertical bars and horizontal bars in element 4 of Group 3 have been clearly distinguished. The proposed method also can reveal some details about element 5 of Group 3 as shown in Figs. 4(c) and 4(d). The proposed method is able to identify the vertical bars in element 5 of Group 3, shown in Fig. 4(c). However, it is difficult to resolve it in element 5 of Group 3 as shown in Fig. 4(d). The proposed method can resolve element 4 of Group 3 with a width of 44.19 μm (close to theoretical limit of 40.0 μm), and is experimentally demonstrated to enable high-resolution imaging through dynamic and complex scattering media. Section 2 in Supplement 1 describes the reconstruction of Group 1, Group 2 and Group 3 using the proposed method and conventional GI, when increased volumes of milk were dropped into water tank and the stirrer operated at 500 rpm. Conventional GI is not applicable, and the proposed method performs well for imaging through dynamic and complex scattering media owing to self-correction.

The 3D-printed transparent samples are also tested as shown in Fig. 5. The same scattering environment is used to test four samples in Figs. 5(a1)–5(a4) and 5(b1)–5(b4). For the four samples in Figs. 5(c1)–5(c4) and 5(d1)–5(d4), dynamic and complex scattering media are formed by dropping different volumes of milk into water tank. As shown in Figs. 5(a1)–5(a4) and 5(c1)–5(c4), it is demonstrated that self-correction of dynamic scaling factors is feasible for high-resolution imaging through dynamic and complex scattering media, and a denoising operation (e.g., BM3D algorithm [44]) has been further applied. However, conventional methods are not feasible for imaging through dynamic and complex scattering media as shown in Figs. 5(b1)–5(b4) and 5(d1)–5(d4).

Optics EXPRESS

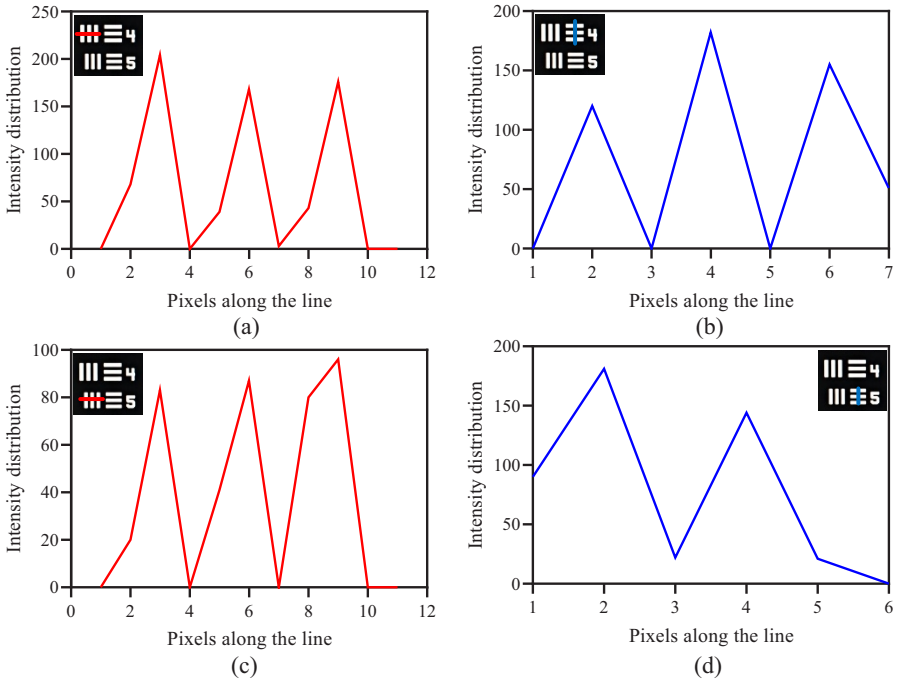

Fig. 4. Intensity distributions of one-dimensional profiles (marked with red and blue lines) in the resolution target recovered by the proposed method (i.e., element 4 of Group 3 and element 5 of Group 3): (a) Intensity distribution of one-dimensional profile marked with a red line within the recovered resolution target (i.e., vertical bars in element 4 of Group 3). (b) Intensity distribution of one-dimensional profile marked with a blue line in the recovered resolution target (i.e., horizontal bars in element 4 of Group 3). (c) Intensity distribution of one-dimensional profile marked with a red line in the recovered resolution target (i.e., vertical bars in element 5 of Group 3). (d) Intensity distribution of one-dimensional profile marked with a blue line in the recovered resolution target (i.e., horizontal bars in element 5 of Group 3). The inset on the top corner is original image only for better visualization and marking.

3.2. *Analysis and discussion*

Figure 6(a) shows a typical example of nonlinear variations of scaling factors induced by using 10 ml milk continuously dropped into water tank and the stirrer at 300 rpm over 4000 seconds. The sample is Group 1 of USAF 1951 resolution target. Although each designed illumination pattern conforms to a rule with the same sum of all pixel values, scaling factors still change due to dynamic and complex scattering media. As can be seen in Fig. 6(a), scaling factors change dynamically. The curve of scaling factors shows a downward trend with nonlinear variations.

Different parameters are also studied as shown in Figs. 6(b)–6(d), i.e., different volumes of milk dropped into water tank, rotation speed of the stirrer and separation distance between object and reference beams. Figure 6(b) shows quality of the reconstructed samples quantified by visibility [45] with different volumes of milk, when the stirrer operates at 500 rpm. The visibility is calculated by

$$\text{visibility} = \frac{<I_s> - <I_b>}{<I_s> + <I_b>}, \tag{8}$$

where I_s and I_b denote intensity distributions in signal part and background part, respectively. The signal part corresponds to effective information about sample, and background part corresponds

Optics EXPRESS

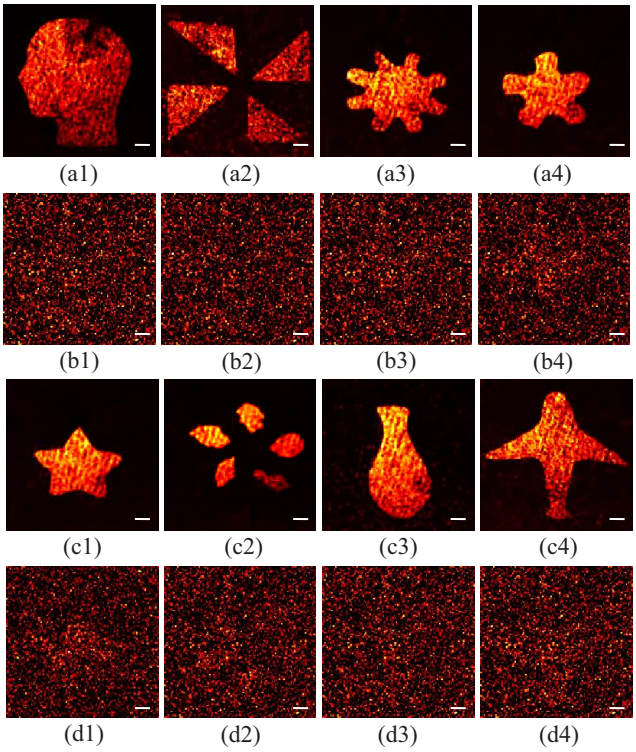

Fig. 5. Reconstruction of 3D-printed transparent samples: (a1)-(a4) and (b1)-(b4) Four samples recovered by the proposed method and conventional GI with 5 ml milk continuously dropped into water tank and the stirrer at 500 rpm, respectively. (c1)-(c4) and (d1)-(d4) Four transparent samples respectively recovered by the proposed method and conventional GI when 5 ml, 5 ml, 6 ml and 4 ml milk are respectively dropped into water tank. Dimensions of feature parts of 3D-printed transparent samples are 6.0 mm × 9.0 mm, 8.0 mm × 8.0 mm, 6.0 mm × 6.0 mm, 6.0 mm × 6.0 mm, 5.0 mm × 5.0 mm, 7.0 mm × 7.0 mm, 4.0 mm × 8.0 mm and 9.0 mm × 8.0 mm, respectively. Scale bar: 1 mm.

to a region without effective information about sample. The average intensity is denoted as $< I_s >$ and $< I_b >$, respectively. The experimental results demonstrate that visibility of the recovered samples stabilizes at 0.8, revealing that the proposed method possesses high robustness against the increased volumes of milk. Conventional GI cannot work with a sharp decline of visibility (from 0.8 to nearly 0), when the volume of milk increases from 0 ml to 20 ml.

Different rotation speeds of the stirrer are also investigated, as shown in Fig. 6(c). With an increase of rotation speed of the stirrer from 100 rpm to 1100 rpm, visibility of sample images recovered by using the proposed method maintains steady (~0.9), when 3 ml and 7 ml milk is respectively dropped into water tank. When the total volume of milk is 11 ml, 15 ml or 20 ml, quality of reconstructed samples still increases as the higher rotation speed is used. However, visibility of sample images recovered by using conventional GI is always close to 0. The distance between the reference and object beams is also studied, and experimental results are shown in Fig. 6(d). 20 ml milk is continuously dropped into water tank, and the stirrer operates at 500 rpm over 4000 seconds. When the reference beam and object beam are close, transfer functions can be assumed to be the same (see Section 3 in Supplement 1 for details). The varied scaling factors induced by dynamic and complex scattering media can be effectively eliminated. The shortest distance allowed in the optical setup is 6.0 cm, which is limited by bulk volumes of

Optics EXPRESS

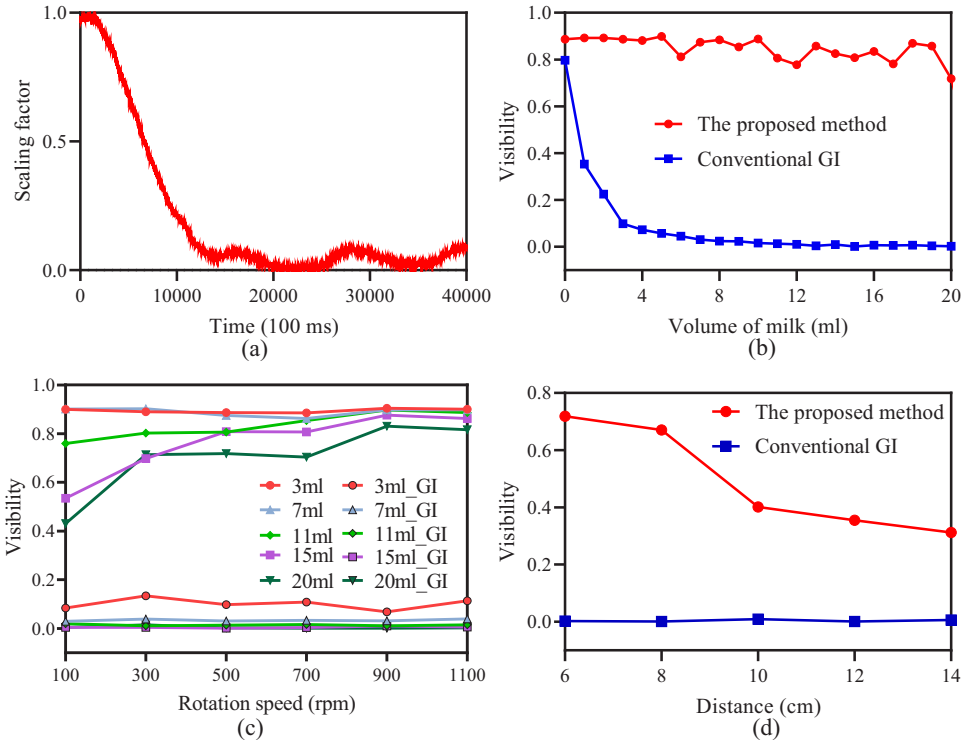

Fig. 6. Properties characterization of the proposed method and conventional GI when Group 1 of USAF 1951 resolution target is used as a target: (a) A typical example of nonlinear variation of scaling factors induced by 10 ml milk continuously dropped into water tank and the stirrer at 300 rpm over 4000 seconds. (b) The influence of volume of milk on visibility of sample images recovered by using the proposed method and conventional GI when the stirrer operates at 500 rpm. (c) The influence of rotation speed of the stirrer on visibility of sample images recovered by using the proposed method (5 upper lines) and conventional GI (5 lower lines). (d) The influence of the distance between two beams on visibility of sample images recovered by using the proposed method and conventional GI with 20 ml milk continuously dropped into water tank and the stirrer at 500 rpm over 4000 seconds.

laboratory equipments and sample size. With the distance of 6.0 cm used in the designed optical setup, spatial resolution achieved is 44.19 μm, which approaches diffraction limit. The proposed method could be influenced by increasing the distance, leading to a decrease of quality as shown in Fig. 6(d). The higher spatial resolution could be achieved by shortening the separation distance between the reference beam and object beam. However, it is impossible for conventional GI to recover any effective information about the test sample through dynamic and complex scattering media. Figure 7 further shows the reconstructed samples using the proposed method and conventional GI with increased distances between object and reference beams, when the total volume of milk is 20 ml. Based on the above analyses, the proposed method is experimentally verified to be robust against dynamic and complex scattering media, and quality of recovered samples is also quantitatively evaluated by contrast-to-noise ratio (CNR) [46] (see Fig. S5 in Supplement 1).

The analyses using Group 3 of USAF 1951 resolution target are further given in Fig. 8, and the results using Group 2 of USAF 1951 resolution target are given in Fig. S6 in Supplement 1. Figure 8(a) shows a nonlinear variation of scaling factors, when 5 ml milk is continuously

Optics EXPRESS

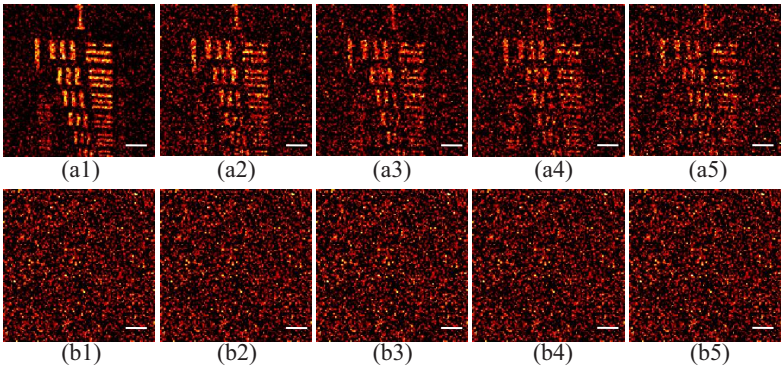

Fig. 7. The reconstructed samples (i.e., USAF 1951 Group 1) obtained by the proposed method and conventional GI with increased distances between object and reference beams when the total volume of milk is 20 ml: (a1)-(a5) The reconstructions using the proposed method with different separation distances (i.e., 6.0 cm, 8.0 cm, 10.0 cm, 12.0 cm and 14.0 cm) and a fixed rotation speed (500 rpm). (b1)-(b5)The reconstructions using conventional GI. Scale bar: 1 mm.

dropped into water tank and the stirrer operates at 500 rpm over 4000 seconds. It can be seen in Fig. 8(a) that scaling factors measured in the reference beam path vary considerably, showing a steeply downward trend in the first 1000 seconds and fluctuating over the last 3000 seconds. The influence of the volume of milk and the rotation speed is shown in Fig. 8(b). Quality of reconstructed samples using conventional GI decreases dramatically with increased volumes of milk regardless of the rotation speeds. The proposed method is able to recover high-resolution samples with visibility of around 0.7, when different volumes of milk (ranging from 0 ml to 7 ml) are respectively dropped into water tank and the stirrer operates at different rotation speeds. Although quality of reconstructed samples using the proposed method would decrease with further increased volumes of milk (e.g., 8 ml and 9 ml), the recovered target can still be well resolved as explained in Section 6 in Supplement 1.

In Fig. 8(c), the horizontal distance is measured between the separatory funnel and reference beam in a range of 12.0 cm to -6.0 cm by moving the separatory funnel closer to reference beam. The horizontal distance of 0 represents that the separatory funnel is right above the reference beam, and negative values denote that the funnel is moved to the left side of the reference beam as shown in Fig. S9 in Supplement 1. The stirrer is not moved in this case. The dynamic and complex scattering media used in Fig. 8(c) is formed by using 9 ml milk and the stirrer at 500 rpm over 4000 seconds. It is demonstrated that visibility of reconstructed samples using the proposed method slightly fluctuate (~0.6), and conventional GI cannot work. The influence of positions of the stirrer is shown in Fig. 8(d), and the distance is denoted between the stirrer and the object beam. More details about the stirrer position are described in Fig. S10 in Supplement 1. The separatory funnel is not moved in this case. The dynamic and complex scattering environment is formed by using 9 ml milk and the stirrer at 500 rpm over 4000 seconds. When position of the stirrer is changed, the proposed self-correction approach is still effective and conventional GI is unable to retrieve the target.

To illustrate the turbidity, mean free path (MFP) [47] is calculated and shown in Fig. 9. The MFP is used and described by

$$\mathrm{MFP} = \frac{1}{\mu}, \tag{9}$$

where μ denotes an extinction coefficient given by

$$I_z = I_0 e^{-\mu z}, \tag{10}$$

Optics EXPRESS

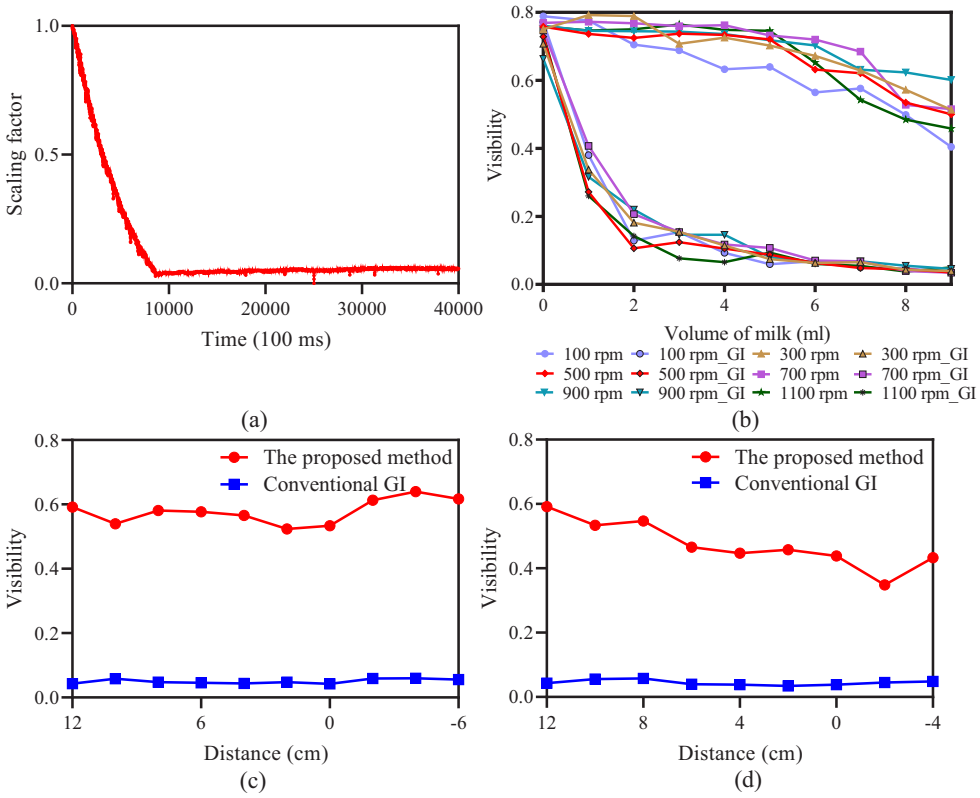

Fig. 8. Properties characterization of the proposed method and conventional GI when Group 3 of USAF 1951 resolution target is tested: (a) A typical example of nonlinear variations of scaling factors induced by 5 ml milk and a stirrer at 500 rpm over 4000 seconds. (b) Influence of the volume of milk and the rotation speed on the proposed method (6 upper lines) and conventional GI (6 lower lines). (c) The influence of horizontal distance between the separatory funnel and reference beam on the proposed method and conventional GI with 9 ml milk and the stirrer at 500 rpm over 4000 seconds. (d) The influence of horizontal distance between the stirrer and the object beam on the proposed method and conventional GI with 9 ml milk and the stirrer at 500 rpm over 4000 seconds.

Optics EXPRESS

where z denotes thickness of scattering media, I_0 denotes initial light intensity at the reference beam path when scattering environment is static without milk, and I_z denotes light intensity at the reference beam path when a certain volume of milk is continuously dropped into water tank and a stirrer rotates at a certain speed.

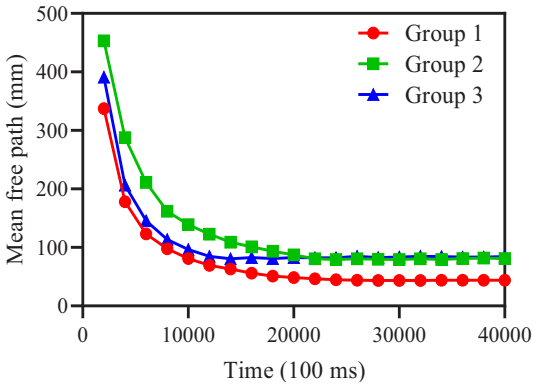

Fig. 9. The MFP changes over time.

As can be seen in Fig. 9, turbidity of scattering environments is changed, which is similar to the trend of scaling factors in Figs. 6(a) and 8(a). With milk continuously dropped into the water tank, turbidity of scattering environment changes. For Group 1, Group 2 and Group 3 of USAF 1951 resolution target, scattering environments are respectively formed by using 20 ml, 8 ml and 9 ml milk continuously dropped into water tank and the stirrer at 1100 rpm over 4000 seconds. With the decreased light intensities recorded in the reference beam path, the MFP keeps decreasing as shown in Fig. 9, and turbidity of dynamic and complex scattering media increases correspondingly. It is illustrated that the decrease of MFP corresponds to an increase of turbidity of scattering media. The details about CNR values of recovered samples (i.e., Group 2 and Group 3 of USAF 1951 resolution target) are given in Section 8 in Supplement 1. It is demonstrated that the proposed method provides a general solution for high-resolution imaging in complex scattering environments.

Based on the above analyses, effectiveness and robustness of the proposed self-corrected optical imaging are demonstrated by using optical experiments through dynamic and complex scattering media. With a parallel detection using dual single-pixel detectors, the proposed method can supervise and self-correct dynamic scaling factors, and can implement high-resolution object reconstruction through dynamic and complex scattering media where conventional methods could not work. The spatial resolution achieved by the proposed method is 44.19 μm, approaching diffraction limit in the designed optical setup. Furthermore, it is experimentally validated that the proposed method shows unprecedented robustness against dynamic and complex scattering media.

4. Conclusion

We have reported a new method, i.e., self-corrected imaging, which allows high-resolution object reconstruction through dynamic and complex scattering media by applying a parallel detection with dual single-pixel detectors. It is experimentally demonstrated that the proposed method enables high-resolution imaging through dynamic and complex scattering media where conventional imaging could not work. The spatial resolution achieved is 44.19 μm, approaching diffraction limit (i.e., 40.0 μm). The achievable spatial resolution is dependent on pixel size of spatial light modulator. Furthermore, the proposed method shows high robustness against dynamic

Optics EXPRESS

and complex scattering media. The proposed self-corrected optical imaging provides a solution for high-resolution object reconstruction in dynamic and complex scattering environments.

Funding. Hong Kong Research Grants Council (C5011-19G, 15224921, 15223522); Hong Kong Polytechnic University (1-W19E, 1-BD4Q).

Disclosures. The authors declare no conflicts of interest.

Data availability. Data underlying the results presented in this paper are not publicly available at this time but may be obtained from the authors upon reasonable request.

Supplemental document. See Supplement 1 for supporting content.

References

1. N. Horiuchi, "Computational imaging: colour imaging with single-pixel detectors," Nat. Photonics **7**(12), 943 (2013).
2. S. Li, F. Cropp, K. Kabra, T. J. Lane, G. Wetzstein, P. Musumeci, and D. Ratner, "Electron ghost imaging," Phys. Rev. Lett. **121**(11), 114801 (2018).
3. M. Sun, M. P. Edgar, G. M. Gibson, B. Sun, N. Radwell, R. Lamb, and M. J. Padgett, "Single-pixel three-dimensional imaging with time-based depth resolution," Nat. Commun. **7**(1), 12010 (2016).
4. D. Pelliccia, A. Rack, M. Scheel, V. Cantelli, and D. M. Paganin, "Experimental x-ray ghost imaging," Phys. Rev. Lett. **117**(11), 113902 (2016).
5. Y. Bromberg, O. Katz, and Y. Silberberg, "Ghost imaging with a single detector," Phys. Rev. A **79**(5), 053840 (2009).
6. T. B. Pittman, "Optical imaging by means of two-photon quantum entanglement," Phys. Rev. A **52**(5), R3429–R3432 (1995).
7. R. S. Bennink, S. J. Bentley, R. W. Boyd, and J. C. Howell, "Quantum and classical coincidence imaging," Phys. Rev. Lett. **92**(3), 033601 (2004).
8. A. Valencia, G. Scarcelli, M. D'Angelo, and Y. Shih, "Two-photon imaging with thermal light," Phys. Rev. Lett. **94**(6), 063601 (2005).
9. R. S. Bennink, S. J. Bentley, and R. W. Boyd, "Two-Photon' coincidence imaging with a classical source," Phys. Rev. Lett. **89**(11), 113601 (2002).
10. B. I. Erkmen and J. H. Shapiro, "Ghost imaging: from quantum to classical to computational," Adv. Opt. Photonics **2**(4), 405–450 (2010).
11. J. Cheng and J. Lin, "Unified theory of thermal ghost imaging and ghost diffraction through turbulent atmosphere," Phys. Rev. A **87**(4), 043810 (2013).
12. N. D. Hardy and J. H. Shapiro, "Reflective ghost imaging through turbulence," Phys. Rev. A **84**(6), 063824 (2011).
13. S. Sun, W. T. Liu, J. H. Gu, H. Z. Lin, L. Jiang, Y. K. Xu, and P. X. Chen, "Ghost imaging normalized by second-order coherence," Opt. Lett. **44**(24), 5993–5996 (2019).
14. A. Zhang, Y. He, L. Wu, L. Chen, and B. Wang, "Tabletop x-ray ghost imaging with ultra-low radiation," Optica **5**(4), 374–377 (2018).
15. W. Yu, M. Li, X. Yao, X. Liu, L. Wu, and G. Zhai, "Adaptive compressive ghost imaging based on wavelet trees and sparse representation," Opt. Express **22**(6), 7133–7144 (2014).
16. H. Yu, R. Lu, S. Han, H. Xie, G. Du, T. Xiao, and D. Zhu, "Fourier-transform ghost imaging with hard x rays," Phys. Rev. Lett. **117**(11), 113901 (2016).
17. M. Bina, D. Magatti, M. Molteni, A. Gatti, L. A. Lugiato, and F. Ferri, "Backscattering differential ghost imaging in turbid media," Phys. Rev. Lett. **110**(8), 083901 (2013).
18. L. Wang and S. Zhao, "Fast reconstructed and high-quality ghost imaging with fast Walsh-Hadamard transform," Photonics Res. **4**(6), 240–244 (2016).
19. B. Liu, Z. Yang, X. Liu, and L. Wu, "Coloured computational imaging with single-pixel detectors based on a 2D discrete cosine transform," J. Mod. Opt. **64**(3), 259–264 (2017).
20. S. M. Khamoushi, Y. Nosrati, and S. H. Tavassoli, "Sinusoidal ghost imaging," Opt. Lett. **40**(15), 3452–3455 (2015).
21. F. Ferri, D. Magatti, L. A. Lugiato, and A. Gatti, "Differential ghost imaging," Phys. Rev. Lett. **104**(25), 253603 (2010).
22. B. Sun, S. S. Welsh, M. P. Edgar, J. H. Shapiro, and M. J. Padgett, "Normalized ghost imaging," Opt. Express **20**(15), 16892–16901 (2012).
23. W. Wang, X. Hu, J. Liu, S. Zhang, J. Suo, and G. Situ, "Gerchberg-Saxton-like ghost imaging," Opt. Express **23**(22), 28416–28422 (2015).
24. M. F. Duarte, M. A. Davenport, D. Takhar, J. N. Laska, T. Sun, K. F. Kelly, and R. G. Baraniuk, "Single-pixel imaging via compressive sampling: building simpler, smaller, and less-expensive digital cameras," IEEE Signal Process. Mag. **25**(2), 83–91 (2008).
25. D. L. Donoho, "Compressed sensing," IEEE Trans. Inform. Theory **52**(4), 1289–1306 (2006).
26. O. Katz, Y. Bromberg, and Y. Silberberg, "Compressive ghost imaging," Appl. Phys. Lett. **95**(13), 131110 (2009).
27. Y. Liu, J. Suo, Y. Zhang, and Q. Dai, "Single-pixel phase and fluorescence microscope," Opt. Express **26**(25), 32451–32462 (2018).
28. Z. Xu, W. Chen, J. Penuelas, M. Padgett, and M. Sun, "1000 fps computational ghost imaging using LED-based structured illumination," Opt. Express **26**(3), 2427–2434 (2018).

Optics EXPRESS

29. E. Hahamovich, S. Monin, Y. Hazan, and A. Rosenthal, "Single pixel imaging at megahertz switching rates via cyclic Hadamard masks," Nat. Commun. **12**(1), 4516 (2021).
30. G. M. Gibson, S. D. Johnson, and M. J. Padgett, "Single-pixel imaging 12 years on: a review," Opt. Express **28**(19), 28190–28208 (2020).
31. N. Radwell, S. D. Johnson, M. P. Edgar, C. F. Higham, R. Murray-Smith, and M. J. Padgett, "Deep learning optimized single-pixel LiDAR," Appl. Phys. Lett. **115**(23), 231101 (2019).
32. S. Jiao, J. Feng, Y. Gao, T. Lei, Z. Xie, and X. Yuan, "Optical machine learning with incoherent light and a single-pixel detector," Opt. Lett. **44**(21), 5186–5189 (2019).
33. L. Olivieri, J. S. T. Gongora, L. Peters, V. Cecconi, A. Cutrona, J. Tunesi, R. Tucker, A. Pasquazi, and M. Peccianti, "Hyperspectral terahertz microscopy via nonlinear ghost imaging," Optica **7**(2), 186–191 (2020).
34. R. I. Stantchev, X. Yu, T. Blu, and E. Pickwell-MacPherson, "Real-time terahertz imaging with a single-pixel detector," Nat. Commun. **11**(1), 2535 (2020).
35. R. I. Stantchev, B. Sun, S. M. Hornett, P. A. Hobson, G. M. Gibson, M. J. Padgett, and E. Hendry, "Noninvasive, near-field terahertz imaging of hidden objects using a single-pixel detector," Sci. Adv. **2**(6), e1600190 (2016).
36. V. Kumar, V. Cecconi, L. Peters, J. Bertolotti, A. Pasquazi, J. S. T. Gongora, and M. Peccianti, "Deterministic Terahertz wave control in scattering media," ACS Photonics **9**(8), 2634–2642 (2022).
37. V. Cecconi, V. Kumar, A. Pasquazi, J. S. T. Gongora, and M. Peccianti, "Nonlinear field-control of terahertz waves in random media for spatiotemporal focusing," Open Res. Eur. **2**(32), 32 (2023).
38. S. C. Chen, Z. Feng, J. Li, W. Tan, L. H. Du, J. Cai, Y. Ma, K. He, H. Ding, Z. H. Zhai, Z. R. Li, C. W. Qiu, X. C. Zhang, and L. G. Zhu, "Ghost spintronic THz-emitter-array microscope," Light: Sci. Appl. **9**(1), 99 (2020).
39. D. Wu, J. Luo, G. Huang, Y. Feng, X. Feng, R. Zhang, Y. Shen, and Z. Li, "Imaging biological tissue with high-throughput single-pixel compressive holography," Nat. Commun. **12**(1), 4712 (2021).
40. A. P. Mosk, A. Lagendijk, G. Lerosey, and M. Fink, "Controlling waves in space and time for imaging and focusing in complex media," Nat. Photonics **6**(5), 283–292 (2012).
41. I. M. Vellekoop and A. P. Mosk, "Phase control algorithms for focusing light through turbid media," Opt. Commun. **281**(11), 3071–3080 (2008).
42. B. Mastiani, T. L. Ohn, and I. M. Vellekoop, "Scanning a focus through scattering media without using the optical memory effect," Opt. Lett. **44**(21), 5226–5229 (2019).
43. Y. Xiao, L. Zhou, and W. Chen, "High-resolution ghost imaging through complex scattering media via a temporal correction," Opt. Lett. **47**(15), 3692–3695 (2022).
44. K. Dabov, A. Foi, V. Katkovnik, and K. Egiazarian, "Image denoising by sparse 3-D transform-domain collaborative filtering," IEEE Trans. on Image Process. **16**(8), 2080–2095 (2007).
45. R. I. Khakimov, B. M. Henson, D. K. Shin, S. S. Hodgman, R. G. Dall, K. G. H. Baldwin, and A. G. Truscott, "Ghost imaging with atoms," Nature **540**(7631), 100–103 (2016).
46. B. Redding, M. A. Choma, and H. Cao, "Speckle-free laser imaging using random laser illumination," Nat. Photonics **6**(6), 355–359 (2012).
47. B. Liu, F. Wang, C. Chen, F. Dong, and D. McGloin, "Self-evolving ghost imaging," Optica **8**(10), 1340–1349 (2021).